Polymers **2014**, *6*, 1129-1143; doi:10.3390/polym6041129

OPEN ACCESS

polymers

ISSN 2073-4360

www.mdpi.com/journal/polymers

Article

Mechanical Analysis of Stress Distribution in a Carbon Fiber-Reinforced Polymer Rod Bonding Anchor

Peng Feng *, Pan Zhang, Xinmiao Meng and Lieping Ye

Department of Civil Engineering, Tsinghua University, Beijing 100084, China;
E-Mails: zhangpansat@126.com (P.Z.); mengxinmiao123@163.com (X.M.);
ylp@tsinghua.edu.cn (L.Y.)

* Author to whom correspondence should be addressed; E-Mail: fengpeng@tsinghua.edu.cn;
Tel.: +86-10-6277-2456.

Received: 27 December 2013; in revised form: 1 April 2014 / Accepted: 3 April 2014 /
Published: 11 April 2014

Abstract: This paper presents an elastic shear stress distribution theoretical model at the carbon fiber-reinforced polymer (CFRP)-adhesive interface of a single-rod and a multi-rod straight-pipe bonding anchor. A comparison between theoretical and finite element analysis results reveals that the accuracy of the theory can be used to guide the preliminary design of CFRP rod bonding anchors. The mechanical performance of the inner cone bonding anchor for multi-rods are evaluated within different coefficients of friction and inner inclined angles. Numerical results indicate that the straight-parabolic inner cone bonding anchor has a significant effect on reducing the shear force at the loading end.

Keywords: carbon fiber-reinforced polymer (CFRP) rod; stress distribution; bonding anchor; anchorage efficiency

1. Introduction

Carbon fiber-reinforced polymer (CFRP) has a high strength, is light weight, with excellent fatigue performance and non-corrosive properties and is, thus, widely used in the structures of buildings and bridges in various forms. As an effective form of CFRP, pultruded CFRP rods or cables can better utilize the unique advantages mentioned above. A cable composed of CFRP rods, as shown in Figure 1a, is made up of unidirectional carbon fibers and the epoxy resin, manufactured by the pultrusion process.

The section of a CFRP rod by scanning electron microscope (SEM) in Figure 1b shows that the unidirectional fibers are embedded in the polymer resin.

Figure 1. (**a**) A cable composed of carbon fiber-reinforced polymer (CFRP) pultruded rods; (**b**) scanning electron microscope (SEM) image of a rod section.

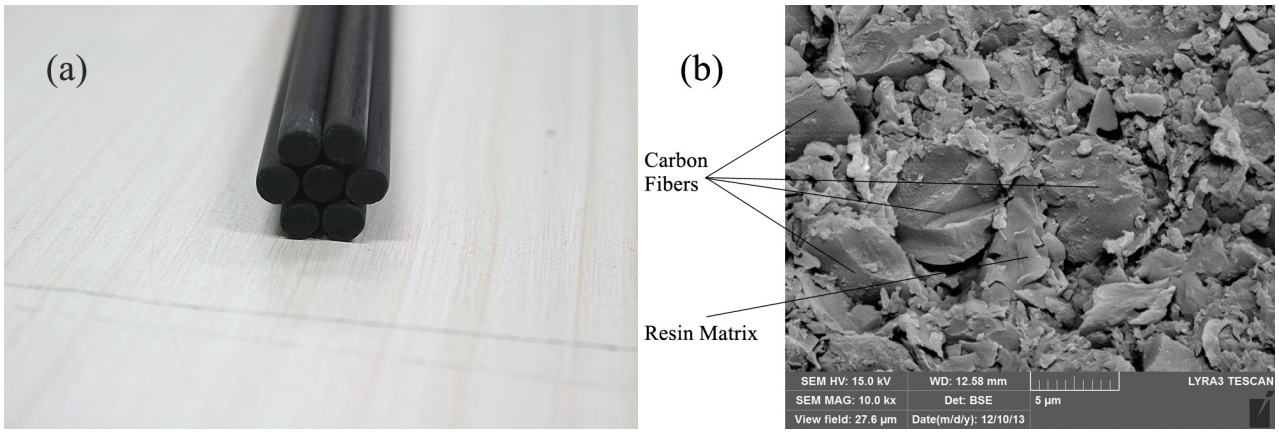

The specific strength of the CFRP cable is fairly high compared to that of a steel cable, while the density of CFRP is one-fourth that of steel. This makes it more suitable for large-span structures, such as large-span roof systems [1–3] and cable-stayed bridges [4,5]. The corrosion of steel cables in the long run can also be avoided by using CFRP cables.

However, the anchorage system is the key factor of whether CFRP cables can reach tensile strength in service. Compared to steel, the anisotropy and brittleness of CFRP make it more difficult to anchor. Currently, anchorage systems can be roughly divided into the clamp anchor, bonding anchor and barrel-wedge anchor [6]. The CFRP rod bonding anchorage system is made up of a metal barrel, CFRP rods and bonding medium, usually epoxy resin or cement grout. The surface of the CFRP rod can be threaded or sandblasted. The anchoring force is via chemical bonding, mechanical interlocking and friction at the interface between the bonding medium and the CFRP rod.

Several CFRP rod anchorage systems were studied. Parametric analysis of the barrel-wedge-type anchor has been reported. A four-wedge type anchor used to grip a single CFRP rod was proposed [7]. The effect of the friction coefficient, the barrel-wedge angle difference and the soft metal sleeve on the stress distribution and stiffness of the anchor was studied [8]. Similar research has shown that the friction coefficient, preload value and sleeve material has a significant effect on the anchorage performance [9–11]. Mayah also mentioned that the use of arc barrel-wedge surfaces with varying inclined angles in a longitudinal direction might reduce concentrated stresses at the loading end [12]. For the bonding anchor, the bond-slip relationship influences the stress distribution along the rod. The bond-slip relationship between the CFRP rod and the cement grout was investigated [13,14], and the results revealed that the surface condition of the rod, the expansion of the cement grout, the anchorage length and the elastic modulus of the barrel can influence the anchorage performance to different degrees.

There is some research on multi-rod anchors, but not as much as single-rod ones, because it is more difficult to grip a collection of rods as opposed to only one. To anchor multiple rods, the bonding anchor is preferred over the barrel-wedge-type anchor. The CFCC (Carbon Fiber Composite Cable)

strand in Japan already has a mature post-tensioning anchorage system using highly expansive cementing material used in the Penobscot Narrows Cable Stayed Bridge [15,16]. However, a reduction in strength may occur due to bending and torsion in the manufacturing process of the CFRP strands, which does not apply to parallel rods. A new way to anchor CFRP parallel rods is by changing the elastic modulus of the adhesive along the barrel [17]. Ceramic particles in different diameters have been mixed into the resin to change the elastic modulus of the adhesive. The modulus was low to high from the loading end to the free end, and the concentrated shear stress was significantly reduced by this method.

Based on the existing research, the bonding stress distribution of CFRP single-rod and multi-rod bonding anchors is analyzed by a theoretical model and a finite element program in this paper.

2. Mechanical Analysis of Shear Stress Distribution

The ultimate loading capacity of a CFRP rod anchor generally depends on the shear stress distribution along the rod. The more uniform the stress distribution, the higher the anchorage efficiency.

A theory was proposed to calculate the ultimate capacity of a straight-pipe bonding anchor [18]. The shear stress distribution along the rod was simplified to three parts. The bearing capacity of each part can be calculated through the integration of shear stress, and thus, the whole capacity of the anchor can be calculated. The error was less than 15% *versus* experimental data. Based on the theory above, a simplified model was suggested, such that each part of the shear stress distribution was considered to be a straight line. The ultimate capacity can be gained in the same way [19].

An elastic theoretical model is proposed in this paper to calculate shear stress referring to [18,19]. It generalizes the regularities of the shear stress distribution at the CFRP-adhesive interface. This theory can calculate the shear stress distribution along a single rod or multiple rods in a straight-pipe bonding anchor within an elastic stage. The fundamental assumptions are listed as follows:

1. All the materials are elastic: the stress state of the anchorage system remains elastic.
2. Deformation of the metal barrel is not considered, because the stiffness of the barrel is much higher than that of the adhesive. Therefore, the internal surface of the barrel is considered fixed.
3. Interface slippage is ignored, so that the displacement compatibility can be founded at the interface between the barrel and adhesive (hereinafter, called the first interface) and the interface between the adhesive and CFRP rods (hereinafter, called the second interface).

Thus, the theory is suitable for preliminary shear stress analysis in an elastic state.

2.1. Single Rod

The cross-section of a single-rod anchor is shown in Figure 2a, and the theoretical model of a single rod is shown in Figure 2b. The length of the anchor is set as l, while the diameter of the CFRP rod and the radial thickness of the adhesive are d and t, respectively.

Tensile load (T_0) is applied at the loading end of the CFRP rod. We assume that the axial displacement of the rod has a uniform distribution in one section that is set as $u(x)$. The axial force distribution is set as $T(x)$. The interfacial shear stress at the first interface and the second interface is

$\tau(x)$ and $\tau_b(x)$, while x represents the axial coordinate. The value is zero at the free end and one at the loading end of the anchor.

Figure 2. (**a**) Cross-section of a single-rod anchor; (**b**) theoretical model of a single rod; (**c**) stress state of a single-rod anchor.

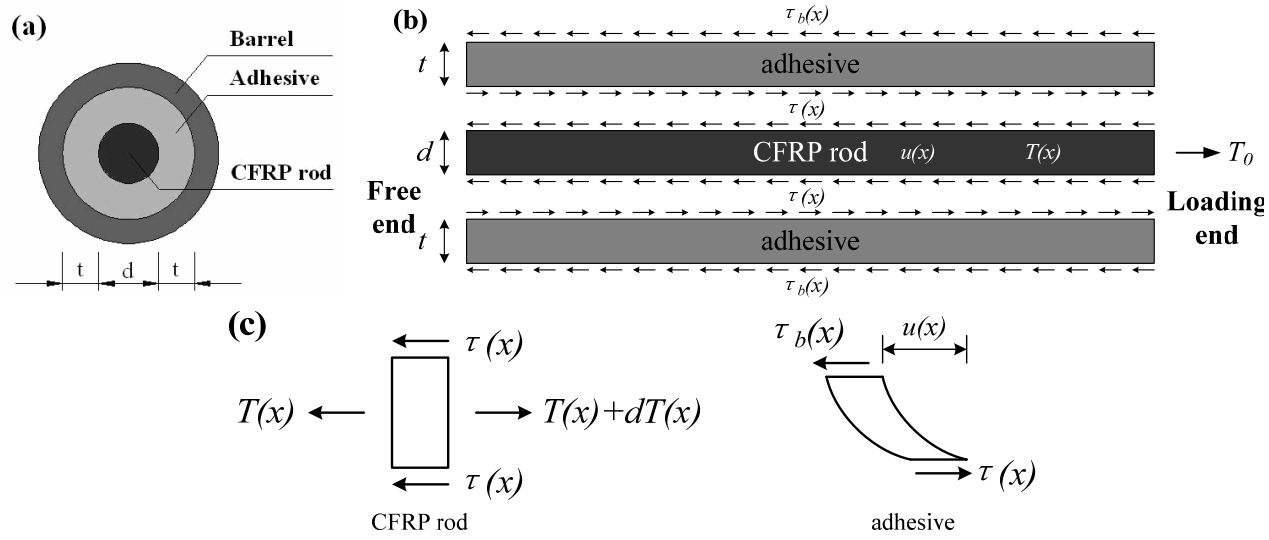

Figure 2c shows the stress state of the CFRP rod and adhesive within infinitesimal length dx in the axial direction. For the CFRP rod, the equilibrium and geometric equation is easily obtained:

$$\tau(x) = \frac{1}{\pi d}\frac{dT(x)}{dx} \tag{1}$$

$$T(x) = E_c A\frac{du(x)}{dx} \tag{2}$$

E_c is the longitudinal elastic modulus of the CFRP rod, and A is the section area. For the adhesive, shear stress at the first and second interface can be considered equilibrant forces to obtain Equation (3):

$$\pi d\tau(x)dx = \pi(d+2t)\tau_b(x)dx \tag{3}$$

Assuming that the shear strain has a linear distribution in the radial direction, the average shear strain of the adhesive can be gained with Equation (3):

$$\bar{\gamma}(x) = \frac{1}{2G}[\tau(x)+\tau_b(x)] = \frac{d+t}{d+2t}\frac{\tau(x)}{G} \tag{4}$$

Here, G represents the shear modulus of the adhesive. The relative displacement between the first and second interface is $u(x)$, and therefore, we can get the geometric equation of adhesive with Equation (4):

$$\frac{u(x)}{t} = \bar{\gamma}(x) = \frac{d+t}{d+2t}\frac{\tau(x)}{G} \tag{5}$$

With Equations (1), (2) and (5) and setting $u(x)$ as the variable, we get a differential equation that is satisfied at any infinitesimal point:

$$u''(x) - k^2 u(x) = 0 \tag{6}$$

In Equation (6), $k^2 = \frac{d+2t}{d+t}\frac{4G}{E_c dt}$. The general solution of Equation (6) is $u(x) = C_1 e^{x} + C_2 e^{-x}$. With boundary conditions at the free end of $u(0) = 0$ and the loading end $T(l) = T_0$, the value of C_1 and C_2 can be calculated as below:

$$C_1 = \frac{d+t}{d+2t}\frac{T_0 kt}{\pi Gd(e^{kl} + e^{-kl} - 2)}; C_2 = -\frac{d+t}{d+2t}\frac{T_0 kt}{\pi Gd(e^{kl} + e^{-kl} - 2)} \quad (7)$$

Therefore, the shear stress distribution can be gained:

$$\tau(x) = \frac{d+2t}{d+t}\frac{G}{t}(C_1 e^{x} + C_2 e^{-x}) \quad (8)$$

2.2. Multiple Rods

The stress distribution in multiple rods can also be derived from theory. A common arrangement is multiple rods symmetrically anchored with one rod in the center and other rods arranged in a ring (Figure 3a). The diameter of the rods is *d*. The radial thickness of the adhesive between the center rod and the side rods is t_1, while it is t_2 between side rods and the barrel. The other parameters are the same as the single-rod anchor system described in Section 2.1.

Figure 3. (**a**) Cross-section of a multi-rod anchor; (**b**) stress state of a multi-rod anchor.

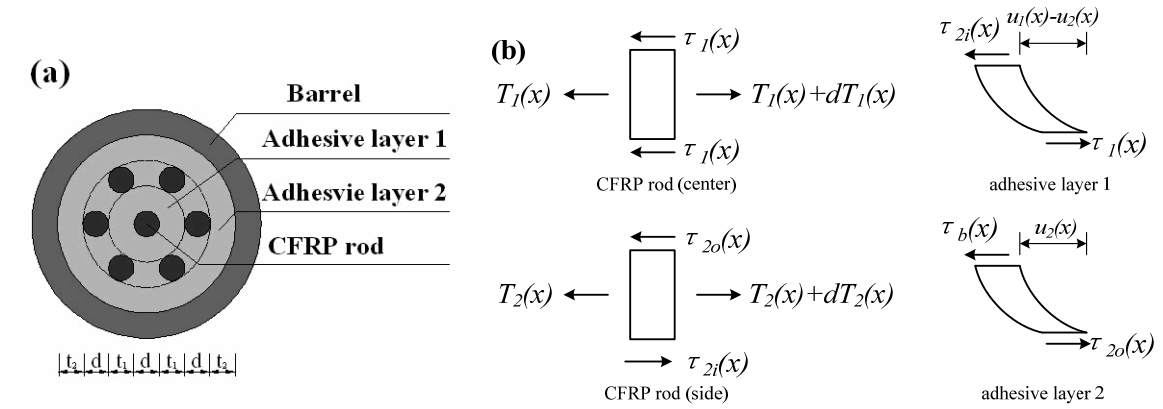

In contrast to the single rod, the shear stress distribution on the surface of the side rods is not uniform along the perimeter. To simplify the theory, the adhesive is considered to be two layers of concentric rings, and the shear stress on the side rods is divided into the inner stress distribution, $\tau_{2i}(x)$, and the outer stress distribution, $\tau_{2o}(x)$. Stress along the center rod is set as $\tau_1(x)$. Axial displacements of the center rod and side rods are expressed as $u_1(x)$ and $u_2(x)$, while the axial forces are $T_1(x)$ and $T_2(x)$. The stress state of the CFRP rod and adhesive within an infinitesimal length is shown in Figure 3b.

According to the equilibrium and interaction relationships from Figure 3b, the inner shear stress distribution on the side rods is in the opposite direction to the others. This indicates that the stress state of multi-rod anchors is more complicated than the single-rod case. The equilibrium and geometric equations for the center rod and side rods can also be described.

$$\begin{gathered}\tau_1(x)=\frac{1}{\pi d}\frac{dT_1(x)}{dx};T_1(x)=E_cA\frac{du_1(x)}{dx};\\ \frac{\tau_{2o}(x)-\tau_{2i}(x)}{2}=\frac{1}{\pi d}\frac{dT_2(x)}{dx};T_2(x)=E_cA\frac{du_2(x)}{dx}\end{gathered} \tag{9}$$

Through simplification, we get:

$$E_cA\frac{d^2u_1(x)}{dx}=\pi d\tau_1(x) \tag{10}$$

$$E_cA\frac{d^2u_2(x)}{dx}=\frac{\pi d}{2}[\tau_{2o}(x)-\tau_{2i}(x)] \tag{11}$$

The shear force for each layer of adhesive is also considered to be approximately equal:

$$\pi d\tau_1(x)dx=\pi(d+2t_1)\tau_{2i}(x)dx \tag{12}$$

$$\pi(3d+2t_1)\tau_{2o}(x)dx=\pi(3d+2t_1+2t_2)\tau_b(x)dx \tag{13}$$

It can be seen from Figure 3b that the relative shear displacement of adhesive Layer 1 is $u_1(x) - u_2(x)$ and $u_2(x)$ for adhesive Layer 2. We can derive the geometric equation of the adhesive with Equations (12) and (13) using the method described above:

$$G\frac{u_1(x)-u_2(x)}{t_1}=\frac{\tau_1(x)+\tau_{2i}(x)}{2}=\frac{d+t_1}{d+2t_1}\tau_1(x) \tag{14}$$

$$G\frac{u_2(x)}{t_2}=\frac{\tau_{20}(x)+\tau_b(x)}{2}=\frac{3d+2t_1+t_2}{3d+2t_1+2t_2}\tau_{2o}(x) \tag{15}$$

With Equations (10)–(15), the displacements, $u_1(x)$ and $u_2(x)$, remain as variables to be solved, and Equations (16) and (17) can be obtained:

$$\frac{d^2u_1(x)}{dx^2}=C_1u_1(x)-C_1u_2(x) \tag{16}$$

$$\frac{d^2u_2(x)}{dx^2}=C_2u_1(x)+C_3u_2(x) \tag{17}$$

In the equations above, the coefficients are listed respectively:

$$C_1=\frac{4G}{E_cdt_1}\frac{d+2t_1}{d+t_1},C_2=-\frac{2G}{E_cdt_1}\frac{d}{d+t_1},C_3=\frac{2G}{E_cd}[\frac{3d+2t_1+2t_2}{(3d+2t_1+t_2)t_2}+\frac{d}{(d+t_1)t_1}] \tag{18}$$

With Equations (16) and (17), the displacement can be solved. By eliminating $u_2(x)$, we get:

$$u_1^{(4)}(x)-(C_1+C_3)u_1^{(2)}(x)+C_1(C_2+C_3)u_1(x)=0 \tag{19}$$

The boundary conditions at the free end and the loading end are $u_1(0)=0$, $u_2(0)=0$, $T_1(0)=T_0$ and $T_2(0)=T_0$, which can be converted into conditions that only contain u_1, as listed in Equation (20):

$$u_1(0)=0;u_1'(l)=\frac{T_0}{EA};u_1''(0)=0;\ u_1'''(l)=0 \tag{20}$$

With Equations (19) and (20), $u_1(x)$ can be calculated to find the shear stress distribution.

3. Finite Element Analysis of Shear Stress Distribution

The finite element method was used to study the stress distribution in the CFRP rod bonding anchor and to test the accuracy of the theoretical model. The anchor was modeled by the Solid45 element in ANSYS software, and nodes on the interface were merged, because slippage is not considered.

3.1. Single Rod Anchor

The CFRP rod, adhesive grout and steel tube were modeled, respectively (Figure 4a). Figure 4b shows the finite element model after meshing with a total element number of 192,000.

Figure 4. (**a**) Numerical model of a single-rod anchor; (**b**) meshed finite element model.

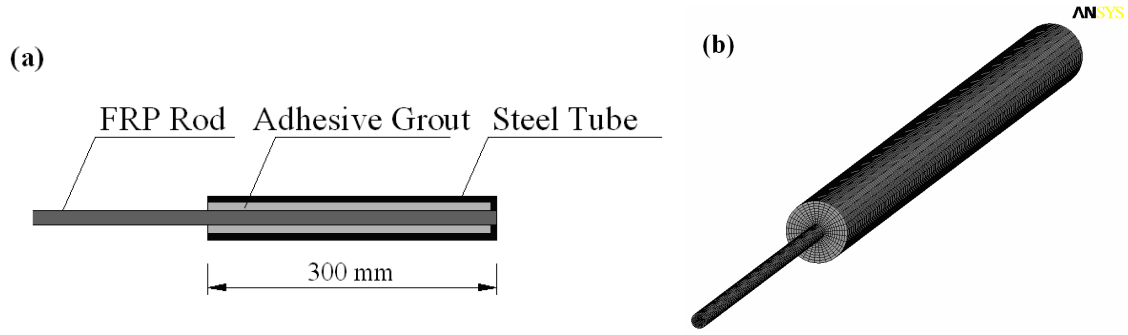

The material properties of CFRP and steel are presented in Table 1. The length of the anchor is 300 mm, and the diameter of the CFRP rod is 5 mm. The thickness of the steel barrel is 2.5 mm. Three kinds of parameter combinations are selected, as shown in Table 2. The elastic modulus and thickness of the adhesives are 5 GPa and 2 mm, 5 GPa and 5 mm and 2 GPa and 5 mm, respectively.

Table 1. Material properties (GPa).

Material	E_x	E_y, E_z	v_{xy}, v_{xz}	v_{yz}	G_{xy}, G_{xz}	G_{yz}
CFRP rod	181	10.05	0.28	0.3	7.17	7.17
Steel	200	/	0.27	/	78.74	/

Table 2. Numerical cases for the single-rod anchor.

No.	1	2	3
Modulus of adhesive (GPa)	5	5	2
Thickness of adhesive (mm)	2	5	5

In the FE (Finite Element) model, the outer surface of the steel tube is restrained in all degrees. A tensile stress of 1500 MPa is then applied to the loading end of the CFRP rod. To compare the numerical and theoretical datasets, each case is also analyzed by theory in Section 2.1. Figure 5a,b displays the displacement and shear stress distribution of the CFRP rod in axial directions by the theory and finite element method. The solid line represents the finite element results, while the dotted line represents the theoretical results. The displacement and stress distribution results generally agree well, while there is some deviation in the shear stress value at the loading end in Figure 5b. This may be caused by stress discontinuity or approximation error in the application of the theory.

From Figure 5a, we notice that the stiffness of the single-rod anchor increases as the modulus of the adhesive increases or the thickness of the adhesive decreases. Figure 5b also shows that the peak value of shear stress increases as the modulus of the adhesive increases or the thickness of the adhesive decreases.

Figure 5. (**a**) Displacement distribution on the rod; (**b**) shear stress distribution on the rod.

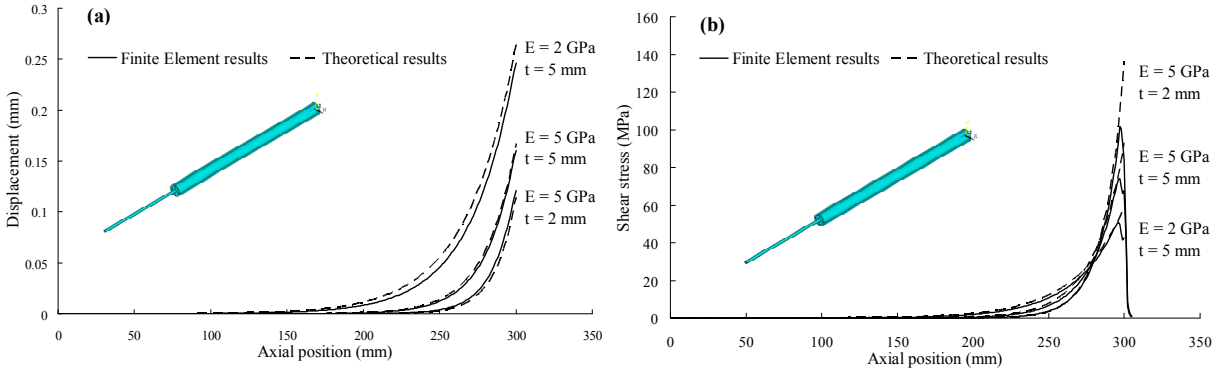

3.2. Multi-Rod Anchor

Figure 6a models a seven-rod bonding anchor with a side view. The rods have a plum-shaped distribution in the adhesive within a certain spacing. There are a total of 245,520 elements after meshing. The material properties of the CFRP and steel are the same as above. The elastic modulus of the adhesive is 5 GPa. The length of the anchor is also 300 mm, and the diameter of the CFRP rod is 5 mm. The outside diameter of the anchor is 45 mm with a 5 mm-thick barrel.

Two kinds of parameter combinations are selected (Table 3). The dimensions of adhesive Layers 1 and 2 are 5 mm + 5 mm and 8 mm + 2 mm, respectively. The outside diameter of the anchor remains constant.

Figure 6. (**a**) Numerical model of a seven-rod anchor; (**b**) meshed finite element model.

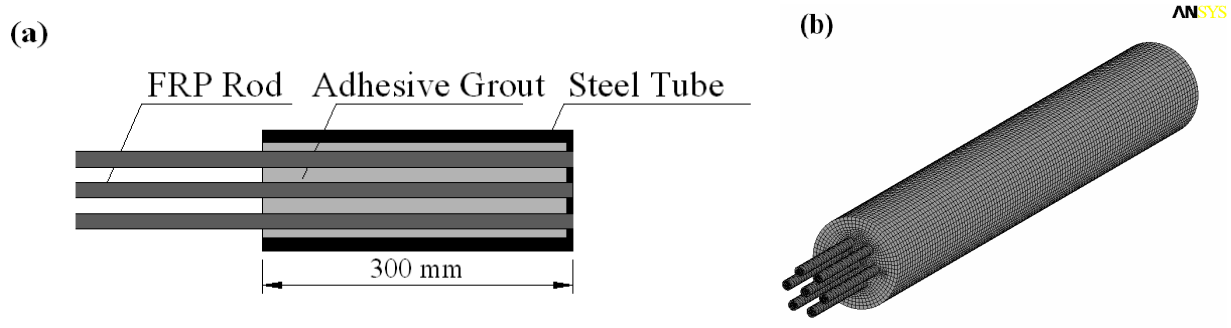

Table 3. Numerical cases for the seven-rod anchor.

No.	Thickness of adhesive Layer 1 (mm)	Thickness of adhesive Layer 2 (mm)
1	5	5
2	8	2

Here, the boundary conditions are the same as the single-rod anchor, and the tensile stress is still set as 1500 MPa on each rod. We used FE to obtain the axial displacement, the shear stress on the surface of the center rod, as well as the shear stress on the inner and outer surface of the side rods.

Mathmetica 6.0 solved differential Equation (19). For each case, the displacement distribution gained by theory and the finite element method is shown in Figure 7a,b, while the shear stress distribution is shown in Figure 8a,b.

Figure 7. (**a**) Displacement distribution of Case 1; (**b**) displacement distribution of Case 2.

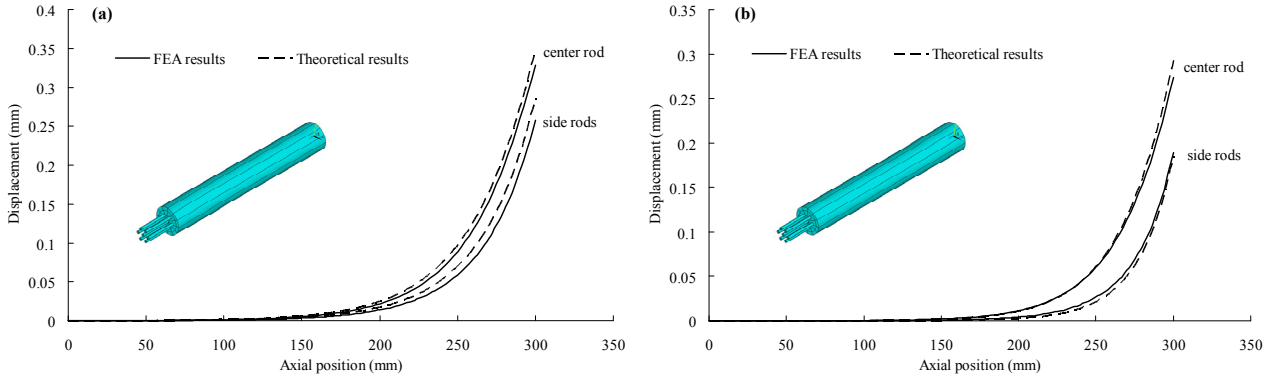

Figure 8. (**a**) Shear stress distribution of Case 1; (**b**) shear stress distribution of Case 2.

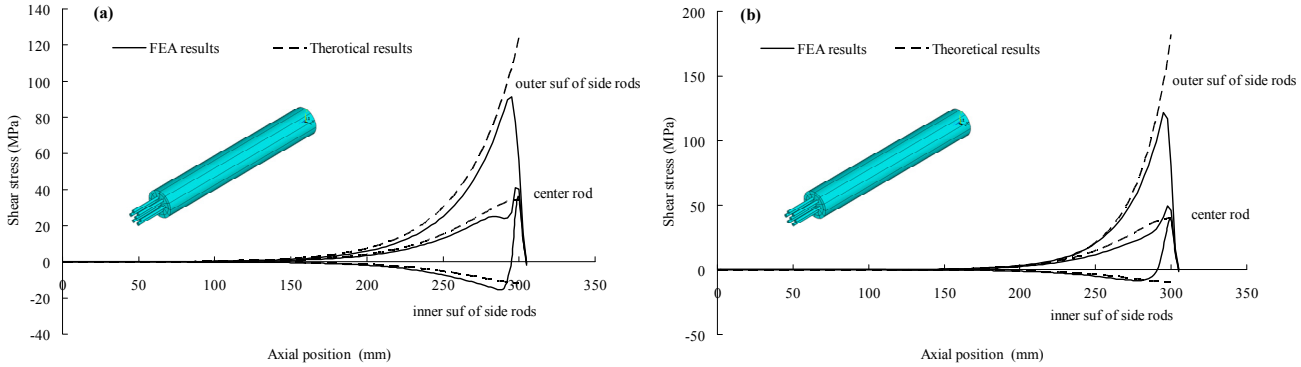

As can be seen, the rod in the center has a shear stress peak with a relatively low value at the loading end. The six rods on the side have a complex shear stress distribution. The shear stress in different positions on the same section of side rods may have opposite directions that are negative inside the rod and positive outside the rod. The peak value is also much bigger than the center rod. As the space between the center rod and side rods increases, the stiffness of the anchor and the shear stress peak increase.

The theoretical and finite element results are generally the same, except for some local positions. Some deviation is seen at the peak point of shear stress close to the end cross-section of the anchorage, and the shear stress on the inner surface of the side rod changes its direction in the FE results. This may be caused by stress discontinuity or approximation error in the application of the theory, which has been explained in Section 3.1. In reality, flexural deformation exists in the side rods, because of an asymmetric stress state, and the stress concentration at the loading end makes the stress state more complicated in this area.

Zhang *et al.* [18] displayed the experimental bond stress distribution of an FRP tendon bond anchorage. The stress peak appears at the loading end when the load is relatively low. Analysis in [19] shows that the shear stress on the side rods is higher than on the center rod. Similar experimental

investigation were conducted on the multiple rod bonding anchor in [20]. The tensile stiffness and the anchorage efficiency is improved when the spacing of the rods gets smaller. Therefore, the experimental results in these references are in good agreement with the theoretical and FE results above.

4. Parametric Analysis of In-Cone Bonding Anchor

A straight-pipe bonding anchor for multiple CFRP rods has some disadvantages (Figure 6). Slippage at the first interface is not allowed, otherwise the rods and adhesive will be pulled out. This leads to a longer bond length and a lower anchorage efficiency [19]. However, the inner cone bonding anchor is more widely used than straight-pipe ones, because radial pressure can be provided at the interface to grip the CFRP rods by an interference fit when slippage occurs at the first interface. Fang *et al*., have studied the inner cone bonding anchors. The loading capacity of the double-rod inner cone anchor filled with RPC (Reactive Powder Concrete) is influenced by the inner inclined angle of the anchor and the rod spacing [21]. The authors also tested the performance of a bonding anchor with nine 12.6 mm-diameter CFRP rods inside [22]. The capacity reduction factor and the critical bond length were discussed through the experimental results.

4.1. Design and Modeling of the Inner Cone Anchor

Additional finite element analysis was performed to investigate the mechanical properties of the inner cone multi-rod bonding anchor. The seven-rod bonding anchor is designed by an anchorage manufacturer in China (Figure 9a) with a 300 mm bond length and a 76 mm outside diameter. The 5 mm-diameter CFRP rods are installed symmetrically in the inner cone barrel by fixtures, and the inner inclined angle is 3%.

Figure 9. (**a**) Primary design of the inner cone bonding anchor; (**b**) 1/6 finite element model.

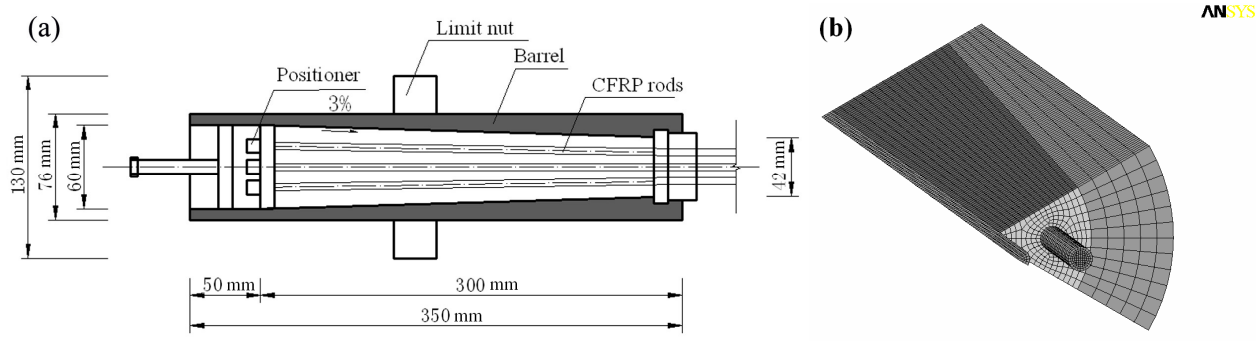

The ANSYS Solid185 element is applied to model the inner cone barrel, adhesive and CFRP rods, and the 1/6 model is shown in Figure 9b with 39,200 elements. The contact element is used at the first interface to permit slippage, while nodes at the second interface are coupled, and thus, the slippage between adhesive and rods is ignored. A tensile load is then applied to seven CFRP rods until the stress of the rods reaches 2000 MPa.

The coefficient of friction (COF) at the first interface and the inner inclined angle were varied to study their influence on the stiffness, radial stress value and shear stress distribution along the rod. The material properties of the rod are the same as in Table 1. The elastic modulus of the adhesive is 5 GPa,

and the yield stress of the steel barrel is 345 MPa. Seven numerical cases are listed in Table 4 with various parameters. Because the change of the inclined angle in the longitudinal direction can reduce the concentrated stress [12], a straight-parabolic inner cone anchor is also added to the inner decline angle group for investigation. The anchor has a straight length of 60 mm from the loading end at the inner surface of the barrel with a 0° angle. The angle then increases along the remaining 240 mm to the free end, where the inner diameter changes parabolically from 42 mm to 60 mm.

Table 4. Numerical cases of the inner cone bonding anchor.

Case No.	1	2	3	4	5	6	7
COF at the first interface	0	0.05	0.1	0.2	0.05	0.05	0.05
Inner inclined angle	3%	3%	3%	3%	2%	4%	Straight-parabolic

4.2. Numerical Results of Inner Cone Anchor

The convergence of the FEM (Finite Element Method) is studied through mesh-refinement of the FE model. The meshing of the straight-parabolic inner cone anchor model is refined with the element number from 39,200 to 148,140. After mesh-refinement, the tensile load value is 50.8 kN when the displacement reaches 15 mm, while it is 50.5 kN in the original model. Under the same stress state of 2000 MPa, the maximum radial compressive stress at the first interface is 111.5 MPa compared to the original value 104.3 MPa. The relative error of the load and stress value is 0.6% and 7%, which is acceptable. Therefore, the convergence of the FEM results is reliable.

The loading curves of the bonding anchor with different first-interface coefficients of friction are illustrated in Figure 10a. The stiffness of the anchor increases when the COF increases from zero to 0.2. As the COF increases, resistance will be stronger while slippage occurs at the first interface. Notice that the load level plateaus and begins to fluctuate when it nears 30 kN. This is because the steel barrel has yielded (equivalent stress reaches 345 MPa in FEA (Finite Element Analysis)), and a higher load capacity cannot be provided. The tensile stress of the rods is 1,300 MPa, which is much lower than the tensile strength. Therefore, the COF at the first interface should not be too low in the anchorage design to avoid the yielding of the barrel and compressive failure of the adhesive. This would lead to a low load capacity.

Figure 10b shows the radial compressive stress distribution at the first interface with different COF values under a certain stress level. The x-coordinate is zero at the free end. The compressive stress value reaches a maximum if there is no friction, with some stress concentration near the loading end, which may be caused by the warping of the adhesive. The stress decreases as the COF increases, because the tensile force is balanced by the horizontal component of the radial compressive and frictional forces. Under a certain tensile load, the frictional force will rise if the COF value increases. This will cause a reduction of compressive force or stress. Therefore, the COF at the first interface should also not be too high, or the radial compression may not be adequate to grip the CFRP rods.

Loading curves with different inner inclined angles are displayed in Figure 11a. As the angle becomes larger from 2% to 4%, the stiffness of the anchor also rises. The straight-parabolic anchor has a stiffness approximately equal to the 3% case. Corresponding to Figure 11a, the radial stress distribution at the first interface under a certain tensile load is illustrated in Figure 11b. The stress

concentration can be observed at the loading end, except for the straight-parabolic case. The stress is higher at the loading end than the free end, and the distribution becomes more uneven when the inclined angle increases. Therefore, increasing the inner inclined angle can improve the stiffness of the anchor, but it also makes the radial stress distribute near the loading end and reduces the effective bond length, which is not expected in the design. Thus, a suitable inclined angle should always be selected.

Figure 10. (**a**) The loading curve of the inner cone anchor with a varying coefficient of friction (COF); (**b**) the radial stress distribution of the inner cone anchor with a varying COF.

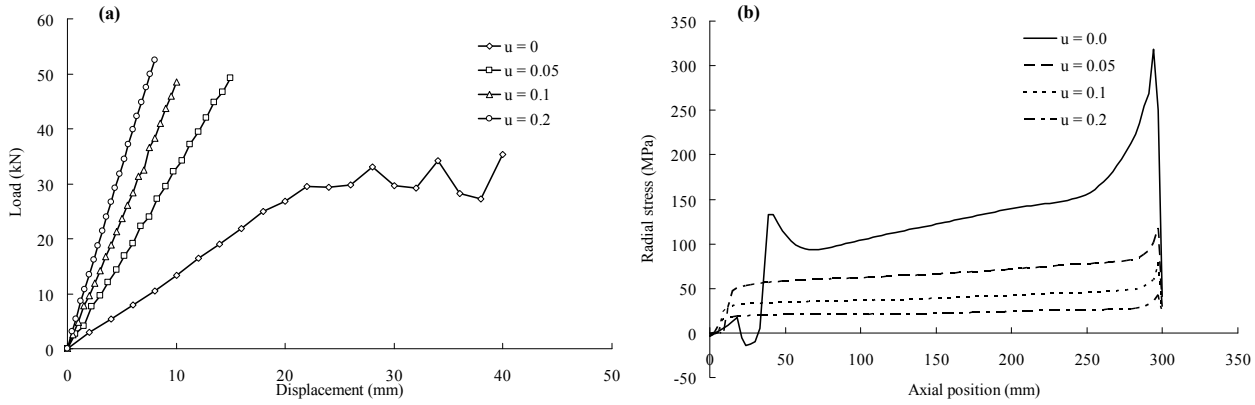

Meanwhile, the radial stress of the straight-parabolic anchor has a larger value at the free end *versus* the loading end. The stress concentration is eliminated due to the 60 mm straight component. A horizontal section of the curve can be observed, because part of the steel barrel has yielded at this point. However, the tensile load can still increase, and premature failure can be avoided, because the yielding of the barrel first occurs at the free end.

Figure 11. (**a**) The loading curve of inner cone anchor with a varying inclined angle; (**b**) the radial stress distribution of inner cone anchor with a varying inclined angle.

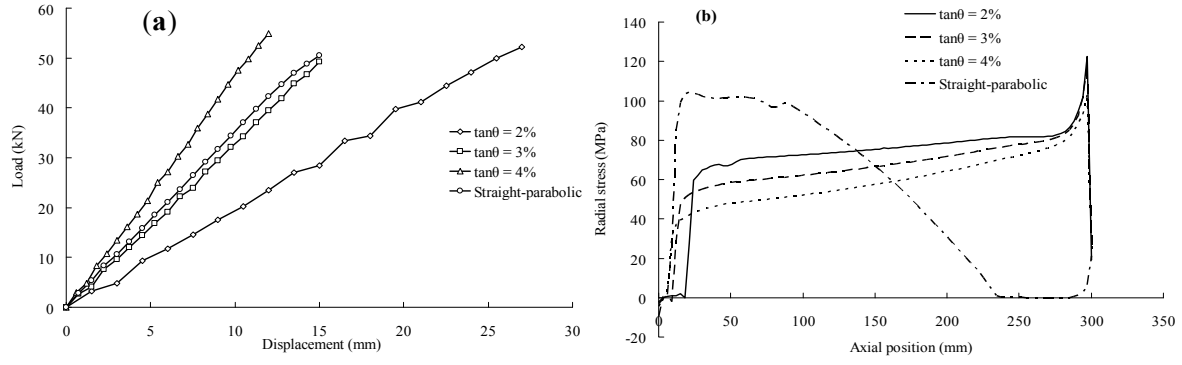

Figure 12 shows the shear stress distribution of Case 2 and Case 7 in Table 4 at the second interface between the CFRP rods and the adhesive for comparison. The shear stress on the surface of the center rod and the inner and outer surface of the side rods is illustrated, respectively. The difference in the stress distribution between the center rod and the side rods has been discussed in Section 3.2. It is not uniform and has a direction opposite that of the inner surface of the side rods. From Figure 12, we can

conclude that the shear stress peak value moves towards the free end in the straight-parabolic anchor *versus* the 3% inclined angle anchor. Thus, the anchorage efficiency can be improved, and the local premature failure of the rods at the loading end can also be prevented.

Figure 12. (**a**) The shear stress distribution of the 3% angle anchor; (**b**) the shear stress distribution of a straight-parabolic angle anchor.

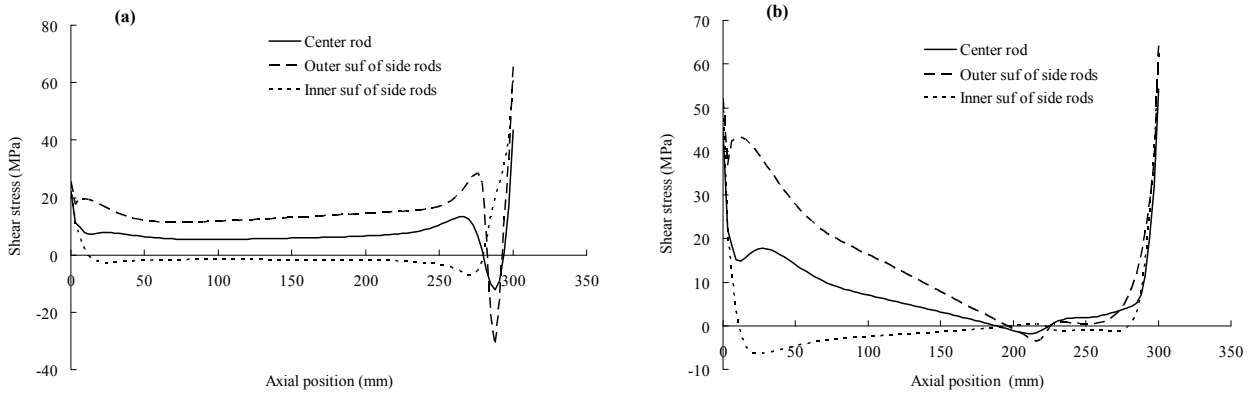

Campell *et al*. [8] did some experiments on the wedge-type anchor, and the results show that the stiffness of the anchorage and radial stress at the barrel-wedge interface increases as the coefficient of friction decreases through greasing. The experimental results of [20] also indicate that the stiffness and loading capacity of the bonding anchor increases as the inclined angle increases from 0° to 3°, which are in good agreement with the FE results above. The radial stress concentration at the loading end of the barrel-wedge anchorage can also be seen in the numerical analysis of [9,11].

5. Conclusions

Based on the research of this paper, the following conclusions can be made:

1. With fundamental assumptions of elasticity and non-slip, a theoretical model for single and multiple rod bonding anchors is proposed by calculating the shear stress distribution on the rods. The theoretical equations are derived from the equilibrium and geometric conditions of the CFRP rods and adhesive. The theoretical model is suitable for preliminary shear stress analysis in the elastic state, and it can provide support for further study on decreasing the shear stress at the loading end cross-section of the anchorage.
2. Finite element results show good agreement with the theoretical results, thus confirming the accuracy of the theory. For the single rod bonding anchor, as the modulus of the adhesive increases or the thickness of the adhesive decreases, the stiffness of the single rod and the peak value of the shear stress will increase. For multi-rod anchors, the stiffness and shear stress peak value will also increase as the space between the center rod and side rods increases. Anyway, the side rods have a complex stress state under tensile force, which may lead to premature failure. Therefore, the modulus and thickness of the adhesive, as well as the space between the rods need to be considered in the anchorage design. The modulus of the adhesive should be high enough to ensure the stiffness of the anchor, but not too high to cause shear or sliding failure. A thin adhesive layer can help to improve the anchorage performance on the condition

that the bond strength is guaranteed. Small spacing between the rods is preferred in a multi-rod anchor, because the longitudinal radial stress is more uniform, and the influence on the side rods caused by asymmetry becomes smaller. The size of the anchorage can also be smaller.

3. In the parametric analysis of the in-cone bonding anchor, as the coefficient of friction at the barrel-adhesive interface increases, the stiffness will increase and the radial compression will decrease, such that it will be more difficult for the steel barrel to yield under a certain load. The stiffness of the anchor also increases when the inner inclined angle increases, with the side effect that the radial pressure is more uneven. In the anchorage design, the inner inclined angle should be appropriate under the overall consideration of the stiffness and radial pressure.
4. Straight-parabolic in-cone anchoring is shown to be an efficient way to reduce the concentrated shear stress and to improve the anchorage efficiency by moving the stress peak from the loading end to the free end. It can be a feasible type of anchorage for CFRP cable made up of parallel CFRP rods in engineering.

Acknowledgments

This work is supported by the China 863 Project (No. 2012AA03A204) and China 973 Project (2012CB026200), and the first author acknowledges the support of Beijing Higher Education Young Elite Teacher Project (YETP0078).

Author Contributions

The work presented here was carried out in collaboration between all authors. Peng Feng, Pan Zhang and Lieping Ye defined the research theme. Peng Feng and Pan Zhang designed the research methods, carried out the finite element analysis and theoretical analysis, analyzed the data and wrote the paper. Xinmiao Meng co-worked on the data collection and their interpretation and presentation. All authors have contributed to, seen and approved the manuscript.

Conflicts of Interest

The authors declare no conflict of interest.

References

1. Feng, P.; Ye, L.P.; Teng, J.G. Large-span woven web structure made of fiber-reinforced polymer. *J. Compos. Constr.* **2007**, *11*, 110–119.
2. Qi, Y.J.; Feng, P.; Ye, L.P. Fundamental mechanical model and analysis of single layer FRP woven web structures. *Eng. Mech.* **2012**, *29*, 180–188. (In Chinese)
3. Qi, Y.J.; Feng, P.; Ye, L.P.; Yang, J.Q. Model test of construction and formation of large-span FRP woven web structures. *J. Build. Struct.* **2012**, *33*, 117–126. (In Chinese)
4. Qi, Y.J.; Feng, P.; Ye, L.P. Comparison of Theoretical Solutions and Ultimate Span-Length between FRP Cables and Steel Cables. *J. Civ. Archit. Environ. Eng.* **2011**, *33*, 52–59. (In Chinese)
5. Wang, X.; Wu, Z.S. Integrated high-performance thousand-metre scale cable-stayed bridge with hybrid FRP cables. *Compos. Part B Eng.* **2010**, *41*, 166–175.

6. Nanni, A.; Bakis, C.E.; O'Neil, E.F.; Dixon, T.O. Performance of FRP tendon-anchor systems for prestressed concrete structures. *PCI J.* **1996**, *41*, 34–43.
7. Sayed-Ahmed, E.Y.; Shrive, N.G. A new steel anchorage system for post-tensioning applications using carbon fiber reinforced plastic tendons. *Can. J. Civ. Eng.* **1998**, *25*, 113–127.
8. Campbell, T.I.; Shrive, N.G.; Soudki, K.A.; Al-Mayah, A.; Keatley, J.P.; Reda, M.M. Design and evaluation of a wedge-type anchor for fibre reinforced polymer tendons. *Can. J. Civ. Eng.* **2000**, *27*, 985–992.
9. Al-Mayah, A.; Soudki, K.A.; Plumtree, A. Experimental and analytical investigation of a stainless steel anchorage for CFRP prestressing tendons. *PCI J.* **2001**, *46*, 88–99.
10. Al-Mayah, A.; Soudki, K.; Plumtree, A. Effect of sandblasting on interfacial contact behavior of carbon-fiber-reinforced polymer-metal couples. *J. Compos. Constr.* **2005**, *9*, 289–295.
11. Al-Mayah, A.; Soudki, K.; Plumtree, A. Effect of sleeve material on interfacial contact behavior of CFRP-metal couples. *J. Mater. Civ. Eng.* **2006**, *18*, 825–830.
12. Al-Mayah, A.; Soudki, K.; Plumtree, A. Novel anchor system for CFRP rod: Finite-element and mathematical models. *J. Compos. Const.* **2007**, *11*, 469–476.
13. Benmokrane, B.; Zhang, B.; Chennouf, A. Tensile properties and pullout behavior of AFRP and CFRP rods for grouted anchor applications. *Constr. Build. Mater.* **2000**, *14*, 157–170.
14. Zhang, B.; Benmokrane, B. Pullout bond properties of fiber-reinforced polymer tendons to grout. *J. Mater. Civ. Eng.* **2002**, *14*, 399–408.
15. Enomoto, T.; Ushijima, K. Use of CFCC tendons and reinforcements in concrete structures for durability. In Proceedings of Asia-Pacific Conference on FRP in Structures (APFIS) 2012, Hokkaido, Japan, 2–4 February 2012.
16. Rohleder, W.J.; Tang, B.; Doe, T.A.; Grace, N.F.; Burgess, C.J. Carbon Fiber-Reinforced Polymer Strand Application on Cable-Stayed Bridge, Penobscot Narrows, Maine. *Transp. Res. Rec. J. Transp. Res. Board* **2008**, *2050*, 169–176.
17. Meier, U. Carbon Fiber Reinforced Polymer Cables: Why? Why Not? What If? *Arab. J. Sci. Eng.* **2009**, *37*, 399–411.
18. Zhang, B.; Benmokrane, B.; Chennouf, A. Prediction of tensile capacity of bond anchorages for FRP tendons. *J. Compos. Constr.* **2000**, *4*, 39–47.
19. Mei, K.H. Analysis of mechanical behavior of CFRP cable bonding anchors. *Bridge Constr.* **2007**, *3*, 80–83. (In Chinese)
20. Zhu, G.P.; Ye, H.W.; Qiang, S.Z. Experimental investigation and mechanical behavior analysis of multiple CFRP tendons anchorage system. *Eng. Mech.* **2011**, *28*, 165–170. (In Chinese)
21. Fang, Z.; Jiang, T.Y.; Liang, D. The Anchorage Behavior of CFRP Tendons in RPC. *J. Hunan Univ.* **2007**, *34*, 1–5. (In Chinese)
22. Fang, Z.; Zhang, K.; Tu, B. Experimental investigation of a bond-type anchorage system for multiple FRP tendons. *Eng. Struct.* **2013**, *57*, 364–373.